Acta Materialia 282 (2025) 120480

Contents lists available at ScienceDirect

Acta Materialia

journal homepage: www.elsevier.com/locate/actamat

A new mechanism for nucleation of $\{11\bar{2}2\}\langle 11\bar{2}3\rangle$ twinning via interaction of $\{11\bar{2}1\}\langle 11\bar{2}6\rangle$ twin variants in hexagonal close-packed metals

Yuyang Wang, Bin Li *, Yiliang Liao

Department of Industrial and Manufacturing Systems Engineering, Iowa State University, Ames, IA 50011, United States

ARTICLE INFO

Keywords:
Deformation twinning
Twin nucleation
Twin-twin interaction

ABSTRACT

Twin nucleation in high symmetry cubic structures is closely related to the activities of dissociated lattice dislocations. However, in low symmetry hexagonal close-packed (HCP) metals, the nucleation mechanisms for deformation twinning remain largely unclear. In this work, we conduct atomistic simulations and uncover a new mechanism for nucleation of $\{11\bar{2}2\}\langle 11\bar{2}3\rangle$ twinning which is an important mode in some HCP metals such as titanium and zirconium. Our simulations show that a coherent $\{11\bar{2}2\}$ twin boundary can be formed as a result of twin-twin interaction between co-zone $\{11\bar{2}1\}$ twin variants. During deformation, three co-zone $\{11\bar{2}1\}$ twins form first and then interact. Two of the $\{11\bar{2}1\}$ twin boundaries (TBs) merge into a coherent $\{11\bar{2}2\}$ TB. This nucleation process does not involve any lattice dislocations or twinning dislocations. Lattice correspondence analyses indicate that such a nucleation process is feasible because all these $\{11\bar{2}1\}$ and $\{11\bar{2}2\}$ twins have the same (0001) K_2 plane. The migration of $\{11\bar{2}2\}$ TB is found to be mediated by the single-layer twinning dislocations.

1. Introduction

Deformation twinning plays a crucial role in the mechanical properties of hexagonal close-packed (HCP) metals and alloys as various twinning modes can be activated during straining. The vector of twinning shear of each twinning mode has a component along the *c*-axis, thus, mechanical twins effectively provide strain accommodation along the *c*-axis which cannot be accomplished by easy dislocation slip systems on the basal and the prismatic planes. The number of easy slip systems fails to meet the von Mises criterion [1] for strain compatibility in polycrystalline metals. In lightweight magnesium (Mg) and its alloys that have been studied extensively over the past two decades, the dominant twinning mode is $\{10\bar{1}2\}\langle 10\bar{1}\bar{1}\rangle$ as profuse $\{10\bar{1}2\}$ twins can be activated during deformation. Another twinning mode, $\{10\bar{1}1\}\langle 10\bar{1}2\rangle$, has also been frequently observed in Mg but with a much lower density. The $\{11\bar{2}1\}\langle 11\bar{2}6\rangle$ and $\{11\bar{2}2\}\langle 11\bar{2}3\rangle$ modes are rarely observed in Mg. In contrast, they are commonly observed in titanium (Ti) and zirconium (Zr) in addition to the $\{10\bar{1}2\}$ and $\{10\bar{1}1\}$ mode [2].

The twinning mechanisms in double lattice HCP structures, in terms of twin nucleation and growth, are more complex than in high symmetry cubic structures and the twinning mechanism significantly differs from mode to mode. In face-centered-cubic (FCC) metals, twin nucleation can be achieved by reaction between two dissociated lattice dislocations. Mahajan and Chin [3] proposed that a three-layer twin embryo could be developed when two dissociated lattice dislocations, i.e., $\frac{1}{2}[0\bar{1}1]\rightarrow\frac{1}{6}[1\bar{2}1]+\frac{1}{6}[\bar{1}\bar{1}2]$ and $\frac{1}{2}[1\bar{1}0]\rightarrow\frac{1}{6}[1\bar{2}1]+\frac{1}{6}[2\bar{1}\bar{1}]$ reacted such that the two identical leading partials, i.e., $\frac{1}{6}[1\bar{2}1]$, were forced to glide on two separate, neighboring (111) planes due to the repulsive force between the partials, and the two trailing partials reacted to form the third twinning partial on top of the first and second twin faults. Based on atomistic simulations, Li et al. [4] modified this mechanism and proposed that the two identical leading partials actually merged into one partial and then the two trailing partials reacted to form a twinning partial that could only glide on a separate, neighboring (111) because of the very high energy barrier for this partial to stay on the original (111) since an A-A stacking sequence would ensue. This way, a two-layer rather than three-layer twin embryo was created by the dislocation reaction. For twin nucleation and growth in body-centered-cubic (BCC) metals, a pole mechanism was proposed by Cottrell and Bilby [5] to describe the dissociation of lattice dislocations and the reaction between the partial dislocations. Although the pole mechanism was never validated by experiments and simulations, twin nucleation and growth in

* Corresponding author.
E-mail address: binl@iastate.edu (B. Li).

https://doi.org/10.1016/j.actamat.2024.120480
Received 13 June 2024; Received in revised form 11 September 2024; Accepted 15 October 2024
Available online 16 October 2024

cubic structure are always closely related to activities of partial dislocations. However, this is not the case for HCP metals.

For twinning modes in HCP metals, the twinning planes are all on the first or second order pyramidal planes. Dislocation slip on these planes, e.g., the $\{10\bar{1}1\}$ and $\{11\bar{2}2\}$, requires a critical stress about two orders of magnitude higher than that of the easy slip systems [6,7]. In fact, profuse $\{10\bar{1}2\}$ twins can be observed shortly after basal slip is activated at a very low stress (on the order of 1.0 MPa [8,9]) in polycrystalline Mg samples. Even though a lattice dislocation may dissociate into a twinning dislocation and a residual dislocation, the magnitude of the Burgers vector of the theoretical twinning dislocations is generally a small fraction of the lattice dislocations. Moreover, the twinning dislocations are typically zonal dislocations that spread over multiple twinning planes [10–12]. Thus, whether twin nucleation is associated with lattice dislocations and how lattice dislocations and other defects facilitate twin nucleation remain largely unclear. Recent studies indicate that there are no well-defined twinning dislocation lines for $\{10\bar{1}2\}$ and $\{11\bar{2}1\}$ twin boundaries (TBs) and only atomic shuffles are involved in twin nucleation and growth [13–18]. This raises an interesting question as to how deformation twins are nucleated in HCP metals. In the literature, there have been very limited studies on the nucleation mechanisms of various twinning modes in HCP metals [19,20].

The initial purpose of this work is to investigate the mobility of a grain boundary (GB) that falls between a $\{11\bar{2}0\}$ and a $\{11\bar{2}2\}$ plane in Mg. These two planes are a pair of corresponding planes in the $\{11\bar{2}1\}\langle 11\bar{2}6\rangle$ twinning mode based on our calculations. Experimental observations and atomistic simulations have shown that when a GB plane falls between two corresponding planes of a twinning mode, the GB has finite mobility [21,22]. For example, the B‖P interface, an interface between the (0001) and $\{10\bar{1}0\}$ which are a pair of corresponding planes of $\{10\bar{1}2\}$ twinning; and the Py‖B interface, an interface between the $\{10\bar{1}1\}$ and (0001) which are a pair of corresponding planes of $\{10\bar{1}1\}$ twinning, have high mobility. Unexpectedly, a new nucleation mechanism for the $\{11\bar{2}2\}\langle 11\bar{2}3\rangle$ twinning mode is revealed as a result of $\{11\bar{2}1\}$ twin-twin interaction. Similar nucleation mechanism is also observed in Ti and in other simulation conditions (Supplemental Material). This mechanism completely differs from the existing dislocation-mediated nucleation mechanisms and provides new insight on how $\{11\bar{2}2\}$ twins are nucleated in HCP metals.

2. Simulation method

The initial configuration of the simulation system before relaxation is shown in Fig. 1a. The Mg bicrystal is comprised of two grains denoted as G1 and G2. These two grains satisfy an orientation relationship (OR) of $(11\bar{2}2)_{G1}\|(11\bar{2}0)_{G2}$, with the zone axis along the $[1\bar{1}00]$ direction. To construct the initial bicrystal, we use Atomsk [23], a toolkit for generating lattice structures and crystalline defects, to create the single crystals and then orient them such that the desired (OR) is satisfied. This particular OR is chosen because the $\{11\bar{2}2\}$ and $\{11\bar{2}0\}$ are a pair of corresponding planes in $\{11\bar{2}1\}\langle 11\bar{2}6\rangle$ twinning mode, according to the crystallography-based calculations by Niewczas [24]. For example, GBs between the $\{1\bar{1}00\}$ and (0001) (the so-called $P \parallel B$ interface [25]) have extremely high mobility. These two planes are exactly the corresponding planes in the $\{10\bar{1}2\}\langle 10\bar{1}\bar{1}\rangle$ twinning mode. During twin growth, the TB assumes a morphology that entirely departs from the theoretical $\{10\bar{1}2\}$ twinning plane [26,16], and the actual TB is often a $P \parallel B$ or $B \parallel P$ interface or both rather than a coherent TB. Using *in-situ* transmission electron microscopy (TEM), Liu et al. [21] observed that GBs between the $\{10\bar{1}1\}$ and (0001) (the so-called *Py* ‖ *B* interface), were developed during *c*-axis compression of a Mg single crystal, and this type of GBs had good mobility. It is noted that the $\{10\bar{1}1\}$ and (0001) are exactly a pair of corresponding planes of the $\{10\bar{1}1\}\langle 10\bar{1}\bar{2}\rangle$ twinning mode [12,24].

As shown in Fig. 1a, the simulation system has dimensions of 13.0 nm (W) × 22.5 nm (L) × 51.8 nm (H), containing a total number of 637,284 atoms. Free surfaces are applied to all three dimensions. No periodic boundary conditions (PBC) are applied. In PBC, atoms on the opposite boundaries interact. When a system such as the bicrystal in our simulation lacks periodicity, the interaction of atoms on the opposite boundaries differs from the interaction of the bulk atoms, and unintended internal stresses are produced. This undesirable effect may generate spurious structures in the simulation. The system is first minimized in energy, and then relaxed for 200 ps. The simulation temperature is maintained at 5 K. After the system is relaxed (Fig. 1b), the top and bottom four layers of the system are fixed by imposing zero force and velocity on each of these atoms, and then a compressive strain is created along the normal direction to the $(11\bar{2}2)$ plane by moving the atoms on the top free surface downward at a constant displacement rate of 0.01 nm per ps, corresponding to a strain rate of 1.93×10^8 */sec*.

The Embedded Atom Method (EAM) potential [27–31] developed by Liu et al. [32] for Mg is used for our simulations. This potential has been used in numerous atomistic simulations of dislocation slip and

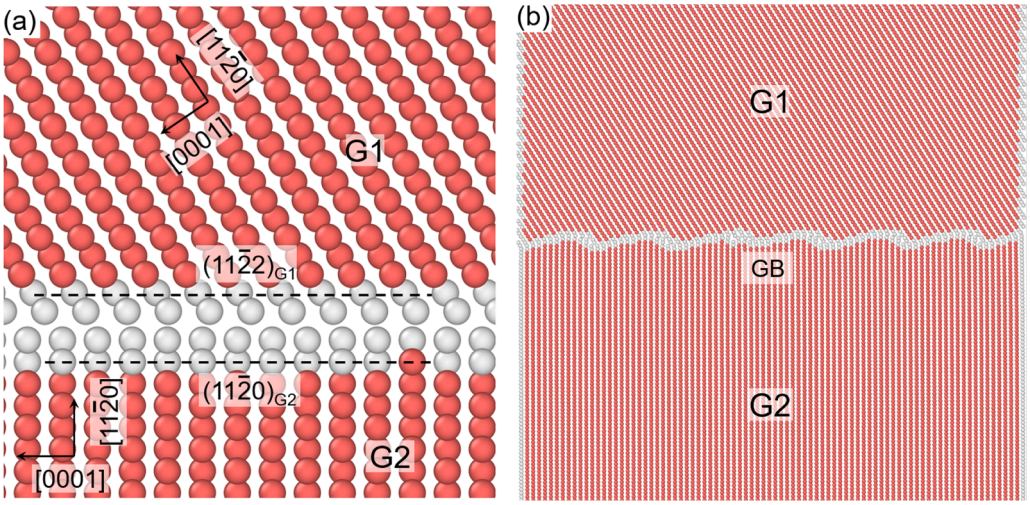

Fig. 1. (a) The initial, unrelaxed configuration of the Mg bicrystal. The grain boundary (GB) is set up such that $(11\bar{2}2)_{G1}\|(11\bar{2}0)_{G2}$, as indicated by the gray atoms. (b) The structure of GB after relaxation. The GB becomes incoherent, consisting of multiple steps. Common neighbor analysis is turned on, where the atoms on the GB are shown in gray.

deformation twinning in Mg [33–35]. In recent years, different types of potentials for Mg have been developed [36–40]. So, we also use other EAM potentials developed by Sun et al. [41] and Wilson et al. [42], as well as the modified embedded-atom method (MEAM) [43] potential created by Kim et al. [44] for our simulations, and similar results are obtained. The visualization toolkit OVITO is used to analyze and trace the evolution of the system during deformation. Common Neighbor Analysis [45] (CNA) is also used to distinguish different crystal structures generated during deformation.

3. Simulation results

After relaxation, the GB evolves into an incoherent morphology with facets along the boundary plane (Fig. 1b). The longer facets are roughly along the $\{11\bar{2}1\}$ plane. The GB energy is ~143 mJ/m^2. Because the average GB plane falls between the two corresponding planes, i.e., $\{11\bar{2}0\}$ and $\{11\bar{2}2\}$, the two grains do not satisfy the $\{11\bar{2}1\}$ twin relationship.

As the compressive strain is increased to a critical value ~3.39%, basal slip is activated first in G1 from the free surface (Fig. 2). Two of the three basal slip systems in G1 have a finite Schmid factor (~0.44), whereas all the basal slip systems of G2 have a zero Schmid factor and no slip can be activated on these planes because the compression direction is perpendicular to the basal normal (Fig. 2a). As the basal dislocation impinges on the GB, further increase in compressive strain leads to the nucleation of a $(11\bar{2}1)$ twin (denoted as $(11\bar{2}1)_{T1}$) which grows from the GB into G1 (Fig. 2b). Zhang et al. [46] observed similar nucleation behavior in their atomistic simulations where impingement of a basal dislocation on a $\{11\bar{2}2\}$ coherent TB led to nucleation of a $\{11\bar{2}1\}$ twin. The $(11\bar{2}1)$ twin relationship can better be seen when the twin thickens (Fig. 2c). The two twin boundaries (TBs) (denoted as $(11\bar{2}1)_{TB1}$ where the subscript TB1 means the TBs are within G1) are along the $(11\bar{2}1)$ plane of G1. Continuation of the compression results in a fully developed $\{11\bar{2}1\}$ twin inside G1 (Fig. 2d), with one tip terminating at the GB. The $(11\bar{2}1)$ twin inside G1 keeps thickening as the compressive strain further increases. More basal dislocations are nucleated at the junction and glide inside G2.

It is worth noting that in Fig. 2(d), at the impingement of the $(11\bar{2}1)$ twin tip at the GB, the interface (indicated by the black arrow) between the $(11\bar{2}1)$ twin and G2 forms a short, coherent $(11\bar{2}2)$ TB, i.e., the $(11\bar{2}1)$ twin and G2 is at the $(11\bar{2}2)$ twin relationship. More details are shown in Fig. 3 below.

As the compressive strain further increases to 3.87%, another $(11\bar{2}1)$

Fig. 2. Evolution of the bicrystal in time sequence under compression. The loading direction is perpendicular to the GB plane. (a) 190 ps. Basal dislocation slip is first initiated. (b) 193 ps. A $(11\bar{2}1)_{TI}$ twin is nucleated from the GB and grows into G1. The twin boundary (TB) is denoted as $(11\bar{2}1)_{TB1}$. (c) 195 ps. The $(11\bar{2}1)$ twin further grows and thickens and the basal planes inside the twin can now be seen. (d) 198 ps. The $(11\bar{2}1)$ twin is fully developed inside G1. Note that the interface between the $(11\bar{2}1)$ twin and G2 is a $(11\bar{2}2)$ TB.

Fig. 3. (a) Nucleation of a second $(11\bar{2}1)$ twin from the tip of the first one, but it grows into G2. The TB is denoted as $(11\bar{2}1)_{TB2}$. (b) As the $(11\bar{2}1)$ twin in G2 grows, the tip of the first $(11\bar{2}1)$ twin in G1, which is part of the GB, is evolving into a coherent $(11\bar{2}2)$ TB (denoted as $(11\bar{2}2)_{TB2}$), with respect to G2. (c) The coherent $(11\bar{2}2)_{TB2}$ extends further down into G2, forming a special twin configuration: above the GB, the twin is a $(11\bar{2}1)$ twin with respect to G1, whereas across the GB, the same twin is a $(11\bar{2}2)$ twin with respect to G2. The first $(11\bar{2}1)$ twin which is with respect to G1, and the second $(11\bar{2}1)$ twin which is with respect to G2, also satisfy the $(11\bar{2}1)$ twin relationship. (d) Eventually, the second $(11\bar{2}1)$ twin disappears, and two coherent $(11\bar{2}2)$ TBs (denoted as $(11\bar{2}2)_{TB2}$) are formed, both with respect to G2.

twin (denoted as $(11\bar{2}1)_{T2}$) is nucleated at the impingement and grows into G2, as shown in Fig. 3a. This TB is denoted as $(11\bar{2}1)_{TB2}$, meaning the TBs are inside G2. This $(11\bar{2}1)$ twin lengthens and thickens via consuming G2; meanwhile, the $(11\bar{2}1)$ twin inside G1 also thickens and its interface with G2 can now be better visualized, and indeed, the interface is a coherent, mobile $(11\bar{2}2)$ TB (denoted as $(11\bar{2}2)_{TB2}$) as it gradually extends into G2 while both $(11\bar{2}1)$ twins grow in G1 and G2, respectively (Fig. 3b). While the TBs are migrating inside G1 and G2, an interesting feature can now be observed. The interface between $(11\bar{2}1)_{T1}$ and $(11\bar{2}1)_{T2}$ is also a mobile interface that is exactly along the $(11\bar{2}1)$ planes of the two $(11\bar{2}1)$ twins. In other words, the $(11\bar{2}1)_{T1}$ and $(11\bar{2}1)_{T2}$, which are in G1 and G2, respectively, also satisfy the $(11\bar{2}1)$ twin relationship (Fig. 3c). This interface, denoted as $(11\bar{2}1)_{TB}$, is mobile. The top TB between the $(11\bar{2}1)_{T2}$ and GB2 migrates downward, while the $(11\bar{2}1)_{TB}$ migrates upward. When these two mobile TBs eventually meet and merge, the $(11\bar{2}1)_{T2}$ twin is entirely consumed and disappears. As a result, a fully developed $(11\bar{2}2)$ twin is formed inside G2 with both TBs are perfectly coherent on the $(11\bar{2}2)$ plane of G2. Finally, a very interesting twin configuration is developed. Above the GB, a $(11\bar{2}1)_{T1}$ twin is formed in G1; however, this same crystal extends into G2 but its orientation with respect to G2 satisfies the $(11\bar{2}2)$ twin relationship.

Careful examination shows that one-layer steps can be observed on the $(11\bar{2}2)$ TBs (Fig. 3b) and these are one-layer twinning dislocations (TDs) that glide on the $(11\bar{2}2)$ twinning plane. An example of the one-layer TD is displayed in Fig. 4a which is a magnified view of the $(11\bar{2}2)$ TB. The step height equals the interplanar spacing of $(11\bar{2}2)$ twinning plane. Fig. 4b shows a view of the twinning plane along the plane normal. The one-layer TD line can now be observed. A recent study showed that the core zone of the one-layer TD spread because atomic shuffling was involved for the parent atoms to be carried to the twin positions [47].

To better reveal how the $(11\bar{2}2)$ TBs are formed during the interaction of $(11\bar{2}1)$ twins in G1 and G2, we plot the motion of the TB triple junctions that are formed during twin-twin interaction in Fig. 5. As shown in Fig. 3, two of the $(11\bar{2}1)$ TBs merge and grow the $(11\bar{2}2)$ TB. We highlight the three TBs that join and from a tripe junction with the purple lines (Fig. 5a). The $(11\bar{2}1)_{TB2}$ which is the bottom TB of the $(11\bar{2}1)_{T2}$ twin, the $(11\bar{2}1)_{TB}$ which is the interface between the $(11\bar{2}1)_{T1}$

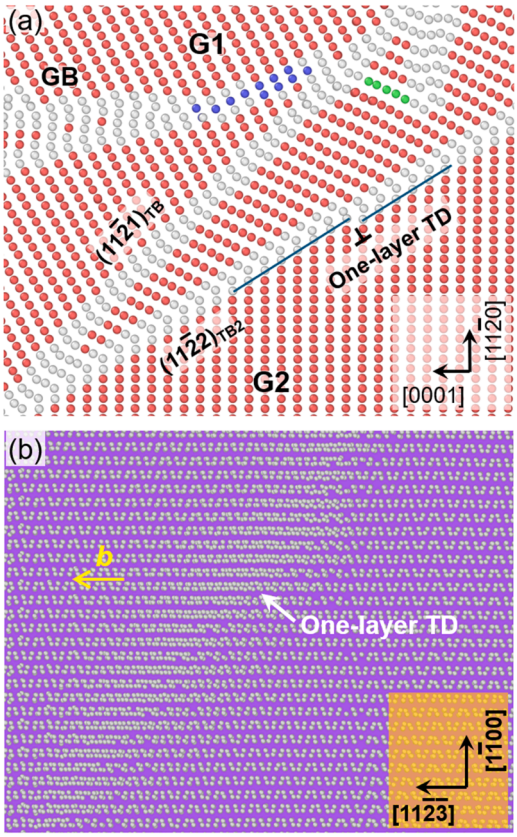

Fig. 4. (a) A magnified view of the structure of the $(11\bar{2}2)$ TB in Fig. 3b. A one-layer twinning dislocation (TD) can be identified. (b) The one-layer TD line when viewed along the normal to the $(11\bar{2}2)$ twinning plane. The glide of the one-layer TDs thickens the $(11\bar{2}2)$ twin.

twin and the $(11\bar{2}1)_{T2}$ twin, and the $(11\bar{2}2)_{TB2}$ meet at TB triple junction I. This triple junction is highly mobile (Fig. 5b). As it moves toward lower left, the $(11\bar{2}2)$ TB lengthens and the $(11\bar{2}2)$ grows into G2. Another TB triple junction is also formed (Fig. 5c). This triple junction is composed of the top $(11\bar{2}1)_{TB2}$, the $(11\bar{2}1)_{TB}$ and the $(11\bar{2}2)$ TB. Again, the $(11\bar{2}1)_{TB2}$ and the $(11\bar{2}1)_{TB}$ merge and the $(11\bar{2}2)$ TB grows at the expense of the $(11\bar{2}1)_{T2}$ twin which eventually disappears.

The nucleation mechanism for $\{11\bar{2}2\}$ twinning via interaction of $\{11\bar{2}1\}$ twins is not only observed with the chosen GB plane and OR, but is also observed in other simulation conditions. We obtain a similar mechanism in single crystal Mg when a tensile strain is applied along the $[11\bar{2}6]$ direction (about 17° away from the *c*-axis). In this case, $\{11\bar{2}1\}$ twin variants are nucleated first, and their interaction facilitates the nucleation of a coherent $\{11\bar{2}2\}$ TB (Fig. S1 in Supplemental Material). Similar twin-twin interaction between $\{11\bar{2}1\}$ twins that gives rise to nucleation of a $(11\bar{2}2)$ twin is also observed in Ti. Details of the twin-twin interaction, migration of the TBs, lattice correspondence analyses are presented in Fig. S2–4 of Supplemental Material.

4. Analysis and discussion

4.1. Lattice transformation analyses

Our simulation results reveal an unusual but interesting scenario of nucleation of $(11\bar{2}1)$ and $(11\bar{2}2)$ twins in pure Mg, although both twinning modes are rarely observed in Mg in experiments. The $(11\bar{2}1)$ twinning mode has been observed and reported in rare-earth containing Mg alloys [48–50] and in atomistic simulations of deformation of single crystal Mg [51,52]. According to Bilby and Crocker [53], Christian and Mahajan [2], the magnitude of twinning shear *s* of $(11\bar{2}1)$ mode equals $\gamma^{-1} = 0.616$ for Mg (γ is the *c*/*a* ratio, 1.624 for Mg), and this value of *s* corresponds to the second invariant plane, i.e., the K_2 plane, (0001). In theory, this twinning mode is mediated by two-layer zonal twinning dislocations. The lattice transformation for this twinning mode is rather simple because the basal (0001) plane of parent is directly transformed into the basal plane of twin without the need of atomic shuffling. However, Minonishi et al. [54] showed that shuffling was needed because the mirror symmetry about the composition plane could not exist and the stacking sequence in the parent and the twin must change. Li and Chen [18] further demonstrated that no coherent $(11\bar{2}1)$ TBs existed, and the TB was no longer a plane but rather a distorted interface zone that spread over multiple $(11\bar{2}1)$ planes. Consequently, no well-defined twinning dislocation lines could be identified.

The value of *s* of the $(11\bar{2}2)$ mode in the classical twinning theory equals $\frac{2(\gamma^2-2)}{3\gamma} = 0.262$ which corresponds to $K_2 = \{11\bar{2}4\}$. This value is rather small as compared to that of the $\{10\bar{1}2\}$ mode ($s = \frac{\gamma^2-3}{\sqrt{3}\gamma} = 0.129$) and the $\{10\bar{1}1\}$ mode ($s = \frac{4\gamma^2-9}{4\sqrt{3}\gamma} = 0.138$). The corresponding twinning dislocation would be a three-layer zonal [2], meaning the twinning dislocation comprises three $(11\bar{2}2)$ planes simultaneously. This indicates that only one-third of the parent atoms are directly sheared to the twin lattice by the homogeneous twinning shear, and complex atomic shuffles should be required for the rest of atoms to transform the parent lattice into the twin lattice. Li et al. [55,47] analyzed the lattice transformation of the $(11\bar{2}2)$ mode and found that the basal (0001) plane of parent would be transformed into three consecutive $\{11\bar{2}1\}$ plane of twin, and a large distortion would be generated to the structural motif of the HCP lattice. In our simulations, rather complex twin-twin interaction and transformation of $(11\bar{2}1)$ twin into $(11\bar{2}2)$ twin occurs. Thus, it is necessary to analyze the lattice transformation during the twinning processes. As pointed out by Christian [56] and Niewczas [24], deformation twinning is a linear mapping of the parent lattice into the twin lattice during which an atomic plane of parent must be transformed into a corresponding plane of twin. Such a lattice mapping can be represented by a second rank tensor which is determined by the choice of the K_2 plane.

Fig. 6a shows our strategy of analyzing the lattice transformation during twin growth and twin-twin interaction. First, we analyze to what corresponding planes the basal (0001) planes in G1 and G2 are transformed during the twinning processes. For this purpose, we select a basal plane in G1 (colored in pink) and a basal in G2 (colored in cyan) (Fig. 6a), respectively. The color of these two basal planes remains unchanged during the simulation. This allows us to track the lattice transformation without ambiguity. After twin nucleation, growth and twin-twin interaction, the basal plane (in pink) of G1 has been transformed into the basal plane of $(11\bar{2}1)_{T1}$. The cyan basal plane in G2 has initially been transformed into the basal of $(11\bar{2}1)_{T2}$, and then transformed into the basal of the $(11\bar{2}2)$ twin (Fig. 6b). Thus, in all these twinning modes, $(11\bar{2}1)$ and $(11\bar{2}2)$, the K_2 plane is always the (0001) basal plane. This analysis contradicts the predicted $\{11\bar{2}4\}$ K_2 plane for the $\{11\bar{2}2\}$ twinning mode in the classical twinning theory [2], but is consistent with the results from the other atomistic simulations [57] which showed that the (0001) basal plane should be the favorable K_2 plane and the twinning dislocation should be a single-layer regular rather than a three-layer zonal twinning dislocation. The overall lattice transformation of the pre-selected (0001) basal plane can be described as:

$$(0001)_{G2} \rightarrow (0001)_{(11\bar{2}1)\ twin} \rightarrow (0001)_{(11\bar{2}2)\ twin}$$

Indeed, the migration of the $(11\bar{2}2)$ TB is mediated by the single-layered twinning dislocation. Careful examination of Fig. 3b, c show

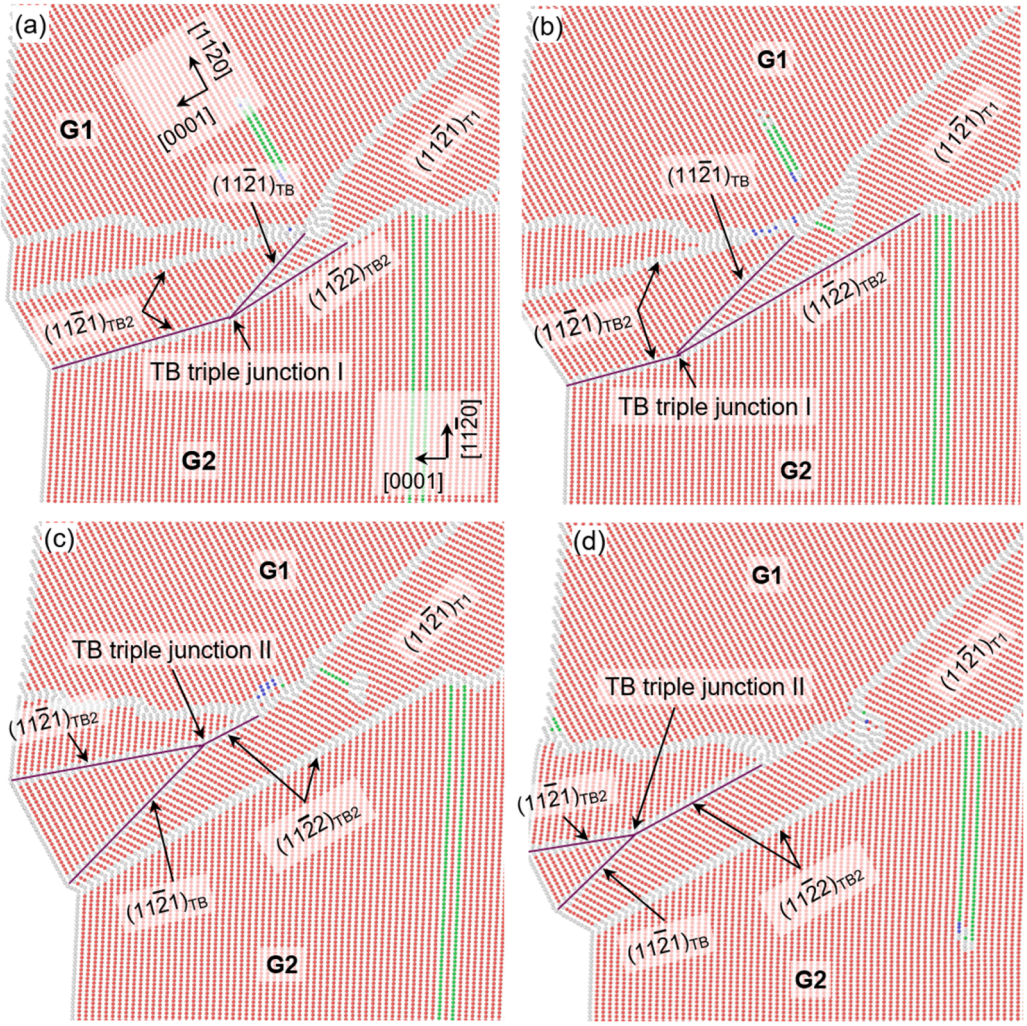

Fig. 5. (a) Formation of twin boundary (TB) tripe junction I. Three TBs (denoted by the purple lines), i.e., the bottom $(11\bar{2}1)_{TB2}$, the $(11\bar{2}1)_{TB}$, and the $(11\bar{2}2)_{TB2}$ meet at the triple junction. (b) The bottom $(11\bar{2}1)_{TB2}$ and the $(11\bar{2}1)_{TB}$ merge such that the bottom $(11\bar{2}2)_{TB2}$ grows and the triple junction I migrates toward lower left. (c) Formation of TB triple junction II. The top $(11\bar{2}1)_{TB2}$ and the $(11\bar{2}1)_{TB}$ merge such that the top $(11\bar{2}2)_{TB2}$ grows and the triple junction II also migrates toward lower left. (d) The $(11\bar{2}2)$ twin grows at the expense of the $(11\bar{2}1)_{T2}$.

that a single-layered twinning dislocation is formed and glides on the $(11\bar{2}2)$ TB.

Next, we analyze the lattice transformation of a $(11\bar{2}4)$ plane in G2. This plane is pre-selected because it was predicted as the K_2 plane of the $\{11\bar{2}2\}$ mode predicted in the classical twinning theory. Similarly, we first select a $(11\bar{2}4)$ plane and color it in dark blue (Fig. 7a). After the growth of the $(11\bar{2}1)_{T2}$ twin in G2, this plane has been transformed into the $(11\bar{2}2)$ plane of the $(11\bar{2}1)_{T2}$ twin (Fig. 7b). Later on, the $(11\bar{2}1)_{T2}$ twin is consumed by the growth of the $(11\bar{2}2)$ twin, and the pre-selected has been transformed into the $(11\bar{2}0)$ plane of the $(11\bar{2}2)$ twin (Fig. 7c). After the disappearance of the $(11\bar{2}1)_{T2}$ twin and the growth of the $(11\bar{2}2)$ twin, the dark blue plane is now entirely residing in the $(11\bar{2}2)$ twin and the corresponding plane can be better identified as $(11\bar{2}0)$ (Fig. 7d). The overall lattice transformation can be described as:

$$(11\bar{2}4)_{G2}\rightarrow(11\bar{2}2)_{(11\bar{2}1)\ T2}\rightarrow(11\bar{2}0)_{(11\bar{2}2)\ twin}$$

Following Niewczas' method [24], we calculated the lattice correspondence of $\{11\bar{2}1\}$ twinning and the results showed that the $(11\bar{2}0)$ and the $(11\bar{2}2)$ were a pair of corresponding planes in this twinning mode. To verify this point, we also conduct the lattice transformation analysis on the $(11\bar{2}0)$ plane in G2 (Fig. 8a). Before deformation, this plane is pre-selected and colored purple. After deformation twinning and twin-twin interaction, this plane has first been transformed into the $(11\bar{2}2)$ plane of the $(11\bar{2}1)_{T2}$ twin, and then transformed into the $(11\bar{2}4)$ of the $(11\bar{2}2)$ twin (Fig. 8b). Thus, indeed, the $(11\bar{2}0)$ plane and the $(11\bar{2}2)$ plane are a pair of corresponding planes in the $\{11\bar{2}1\}$ mode, and this analysis is consistent with our crystallography-based calculations.

4.2. Geometrical analysis in the lattice transformation

As mentioned above, the magnitude of twinning shear s for the $\{11\bar{2}2\}$ mode would equal 0.262 if the K_2 plane were $(11\bar{2}4)$ as predicted by the classical twinning theory. From the lattice transformation analysis in Fig. 6a, the basal plane of G2 is sequentially transformed into the basal of $(11\bar{2}1)_{T2}$ and then into the basal of $(11\bar{2}2)$ twin. Thus, these twins all have the basal K_2 plane. This common feature is crucial and makes possible the sequential lattice transformation. However, the (0001) K_2 plane gives rise to the value of $s=\frac{2}{\gamma}$ which is 1.23. Such a huge s was deemed unfavorable in the classical twinning theory which assumes the magnitude of twinning shear of a twinning mode should be less than 1.0. Most recently, Li et al. [47] conducted scanning transmission electron microscopy (STEM) and atomistic simulation studies on the $\{11\bar{2}2\}$ TB. They found that the migration of TB was indeed

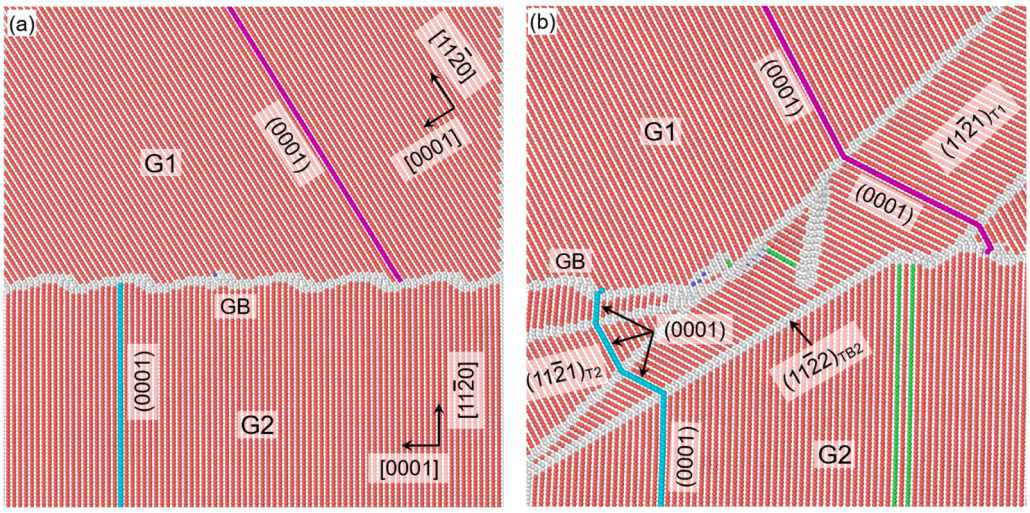

Fig. 6. (a) To perform lattice correspondence analysis, a basal plane in G1 (colored in pink) and a basal plane in G2 (colored in cyan) are pre-selected before compression. (b) After twinning, the pink basal plane of G1 is transformed into the basal plane of the first $(11\bar{2}1)$ twin, indicating the K_2 plane for the $(11\bar{2}1)$ twin is the basal. Meanwhile, the cyan basal plane of G2 is transformed into the basal plane of the second $(11\bar{2}1)$ twin and the $(11\bar{2}2)$ twin, indicating the K_2 plane of these twinning modes is the basal as well.

mediated by the single-layer twinning dislocations, rather than the predicted three-layer zonal twinning dislocations. This single-layer twinning dislocation corresponds to the (0001) K_2 plane. They proposed a half-shear-half-shuffle mechanism to account for the seemingly very large value of *s*. In this mechanism, the single-layer twinning dislocation moves the parent atoms by shear to the midpoint of the overall displacement, and then the parent atoms shuffle to the twin positions. In other words, from the parent lattice to the twin lattice, half of the distance of the parent atoms comes from shearing which is accomplished by the single-layer twinning dislocation, but the other half is accomplished by shuffling. This way, the actual value of *s* is halved. Despite this mechanism of reduced value of *s*, a fairly large strain can be expected in the lattice transformation when the K_2 is (0001) for the $\{11\bar{2}2\}$ mode. In the following, we provide a geometrical analysis on the lattice transformation.

In Fig. 9a, we extract the pre-selected purple $(11\bar{2}0)$ plane of G2, and plot this atomic plane such that the viewing direction is along the plane normal $[11\bar{2}0]$. After the twinning events, this atomic plane spans over regions in G2, the $(11\bar{2}1)_{T2}$ twin and the $(11\bar{2}2)$ twin. The structural change of the pre-selected plane can be seen in Fig. 9b. Apparently, a dimensional stretch has occurred along the [0001] direction, but a structural similarity can still be observed. Such a structural similarity between the corresponding planes of a twinning mode is a manifestation of the principle of lattice transformation in deformation twinning – the parent lattice is linearly mapped into the twin lattice [56]. The boxed region in Fig. 9b is then magnified and plotted in Fig. 9c in which the lattices of G2, the $(11\bar{2}1)_{T2}$ twin and the $(11\bar{2}2)$ twin are colored in purple, red and cyan, respectively. This allows us to compare the lattice strain produced by the $(11\bar{2}1)$ and $(11\bar{2}2)$ twinning.

To quantify the lattice strain induced produced by twinning, two layers of atoms on the $(11\bar{2}0)$, $(11\bar{2}2)$, and $(11\bar{2}4)$ plane are separated and superimposed, as shown in Fig. 10. The initial interatomic spacing between two atoms on the $(11\bar{2}0)$ plane along the [0001] is approximately 5.20 Å. But after the $(11\bar{2}1)$ twinning, the spacing is slightly increased to 6.03 Å. After the $(11\bar{2}2)$ twinning, the spacing is further increased to 8.23 Å. The misfit strain before and after twinning can be expressed as:

$$\varepsilon = \frac{d_{initial} - d_{twin}}{d_{initial}} \quad (1)$$

where $d_{initial}$ is the interatomic spacing on the $(11\bar{2}0)$ plane of G2, and d_{twin} the spacing on the $(11\bar{2}2)$ and $(11\bar{2}4)$ plane after the $(11\bar{2}1)_{T2}$ and $(11\bar{2}2)_T$ twins are formed. The relative misfit strain equals 0.16 between the $(11\bar{2}0)$ and $(11\bar{2}2)$ twinning, 0.36 between the $(11\bar{2}2)$ and $(11\bar{2}4)$ twinning, and 0.58 between the $(11\bar{2}0)$ and $(11\bar{2}2)$ twinning. These values indicate that direct transformation from the $(11\bar{2}0)$ to the $(11\bar{2}4)$ should be rather difficult because a substantial amount of lattice strain would be created. Consequently, nucleation of $\{11\bar{2}2\}$ twins directly from the parent lattice would be difficult. This may explain why nucleation of $\{11\bar{2}2\}$ twins in atomistic simulations from dislocation slip, free surfaces or grain boundaries has not been observed.

4.3. *Nucleation of* $(11\bar{2}2)$ *twinning by twin-twin interaction*

Nucleation of deformation twins in metals is generally preceded by dislocation slip [2]. In high symmetry crystal structures, twin nucleation is associated with the glide of partial dislocations [58]. For instance, in FCC metals, a twin can be considered a pile of planar faults (stacking faults) produced by the Shockley partial dislocations. Thus, twin nucleation and twin growth can be achieved by the glide of identical Shockley partials on consecutive {111} planes. Twin nucleation in FCC metals can also be accomplished by dislocation reaction [3,4]. In high entropy alloys (HEAs) that have very low stacking fault energies and nanograined materials, twin nucleation can also occur by piling up stacking faults that are generated by Shockley partials with different Burgers vectors [59], and in some special twin configurations the overall Burgers vectors add up to zero such that no microscopic shear strain is produced [60,61]. Note that in FCC metals, the twinning plane is also the slip plane of lattice dislocations, but this is not the case in low symmetry HCP metals in which the twinning mechanisms are far more complex.

In HCP metals, all the twinning planes are not the slip systems that have low critical resolved shear stress (CRSS). The easy slip systems, i.e., the (0001) basal and the $\{1\bar{1}00\}$ prismatic slip systems are not twinning planes because these planes already have mirror symmetry and thus a simple shear on the basal or the prismatic planes would disrupt the mirror symmetry and thus cannot produce a twinned structure. Although the $\{10\bar{1}1\}$ and the $\{11\bar{2}2\}$ are both pyramidal slip planes, the Burgers vectors of these pyramidal dislocations, i.e., $\langle c+a \rangle$ are huge if compared with the Burgers vectors of the twinning dislocations, and

Fig. 7. (a) Lattice correspondence analysis for a pre-selected $(11\bar{2}4)$ plane which is blue-colored in G2. (b) As the second $(11\bar{2}1)$ twin is formed, the atoms of the blue $(11\bar{2}4)$ plane are now residing on the $(11\bar{2}2)$ plane of the second $(11\bar{2}1)$ twin. (c) As the $(11\bar{2}1)$ TB between the first and the second $(11\bar{2}1)$ twin migrates and consumes the second $(11\bar{2}1)$ twin, the blue atoms of the $(11\bar{2}2)$ are now residing on the $(11\bar{2}0)$ plane of the $(11\bar{2}2)$ twin. (d) The $(11\bar{2}2)$ twin grows at the expense of the second $(11\bar{2}1)$ twin. All the blue atoms are residing on the $(11\bar{2}0)$ plane of the $(11\bar{2}2)$ twin.

there is no direct connection between twin nucleation and the pyramidal dislocations that are difficult to nucleate and usually do not have a high density during quasistatic deformation of bulk samples. The other two twinning planes, i.e., $\{11\bar{2}1\}$ and $\{10\bar{1}2\}$ are not the slip planes, but the $\{10\bar{1}2\}\langle 10\bar{1}\bar{1}\rangle$ twinning is the most commonly observed mode in all HCP metals. In Mg, the CRSS for $\{10\bar{1}2\}$ twinning is only a few MPa [9] and close to that of the basal slip. Wang et al. conducted density functional theory (DFT) calculations of the energy barrier to $\{10\bar{1}2\}$ twin nucleation and found the value was very low (~27 MeV/atom) [20]. They proposed that nucleation of $\{10\bar{1}2\}$ twins was purely via atomic shuffling. Note that in their work, the atomic shuffles transform the parent basal to the twin prismatic and the parent prismatic to the twin basal, and this lattice transformation is exactly the shuffling dominated mechanism proposed by Li and Ma for the $\{10\bar{1}2\}$ mode [15]. He et al. [62] performed *in-situ* atomic scale HRTEM observations of $\{10\bar{1}2\}$ twinning in rhenium (*Re*). They found that a $\{10\bar{1}2\}$ twin was readily nucleated and grew rapidly via formation of highly incoherent TB that was composed of $\{1\bar{1}00\}_{Parent}\|(0001)_{Twin}$ and $(0001)_{Parent}\|\{1\bar{1}00\}_{Twin}$. These interfaces were called $B \parallel P$ or $P \parallel B$ boundaries. No dislocation activities were involved in the twin nucleation. Despite these observations, dislocation slip, especially those dislocations with a Burgers vector component along the *c*-axis, may be able to facilitate twin nucleation because the elastic strains of the dislocations may effectively accommodate the strains generated by the twin nucleation. TB migration during growth of $\{10\bar{1}1\}\langle 10\bar{1}2\rangle$ twins is mediated by four-layer zonal twinning dislocations which tend to dissociate into two double-layer partial zonal twinning dislocations [12], along with atomic shuffles that are nearly perpendicular to the twinning shear. However, there has been very little discussion on the nucleation mechanism of $\{10\bar{1}1\}$ twins. As to the nucleation of $\{11\bar{2}1\}$ twins, Vaidya and Mahajan [19] proposed that a pyramidal $\langle c+a\rangle = \frac{1}{3}\langle 2\bar{1}\bar{1}3\rangle$ dislocation on the $\{11\bar{2}1\}$ plane could react with two type-$\langle a\rangle$ dislocations, i.e., $\frac{1}{3}\langle 2\bar{1}\bar{1}0\rangle$ and $\frac{1}{3}\langle 1\bar{2}10\rangle$, and form a twelve-layer zonal twinning dislocation. This dislocation reaction creates a twelve-layer twin embryo. This mechanism has not been validated by experiments and simulations.

The geometrical analysis of the lattice transformation (Figs. 9, 10) in the $\{11\bar{2}2\}$ twinning mode suggests that direct transformation from the parent lattice to the twin lattice should be rather difficult because the overall misfit strain is large (~58%), unless a high stress or high stress concentration is present [63]. Thus, one would expect that the $\{11\bar{2}2\}$ twin volume fraction should be very low in deformation of HCP metals. However, this is at odds with the experimental observations. Although rarely observed in Mg, profuse $\{11\bar{2}2\}$ twinning has been observed as commonly as $\{10\bar{1}2\}$ twins in Ti and Zr. High density $\{11\bar{2}2\}$ twins were

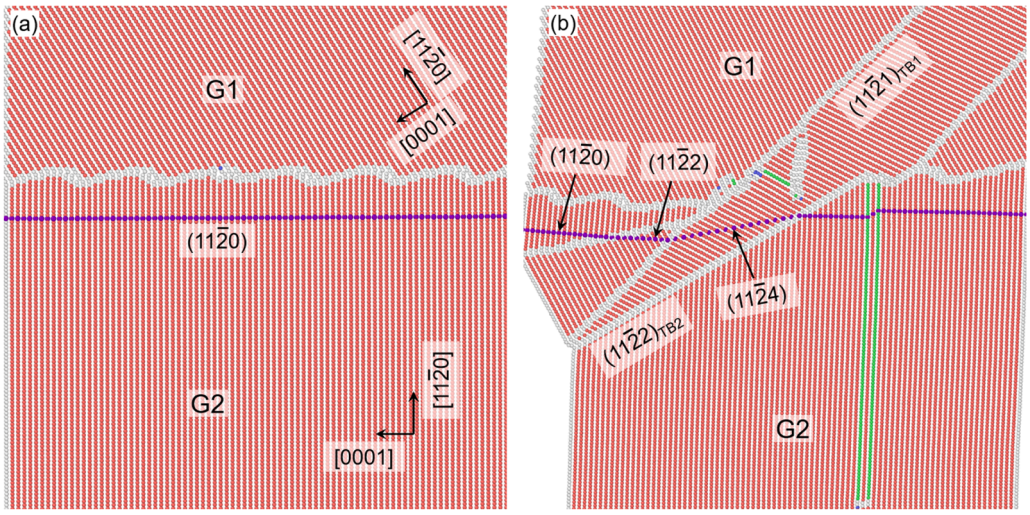

Fig. 8. (a) A (11$\bar{2}$0) prismatic plane in G2 is pre-selected and colored in purple to analyze the lattice transformation during serial twinning. (b) Across the coherent (11$\bar{2}$2) TB, the (11$\bar{2}$0) plane is transformed into the (11$\bar{2}$4) plane of the (11$\bar{2}$2) twin. Between the (11$\bar{2}$2) twin and the second (11$\bar{2}$1) twin in G2, the lattice correspondence can be described as (11$\bar{2}$2)→(11$\bar{2}$4). Between G2 and the second (11$\bar{2}$1) twin in G2, the pre-selected (11$\bar{2}$0) plane is transformed into the (11$\bar{2}$2). The serial lattice transformation can be described as (11$\bar{2}$0)→(11$\bar{2}$2)→(11$\bar{2}$4).

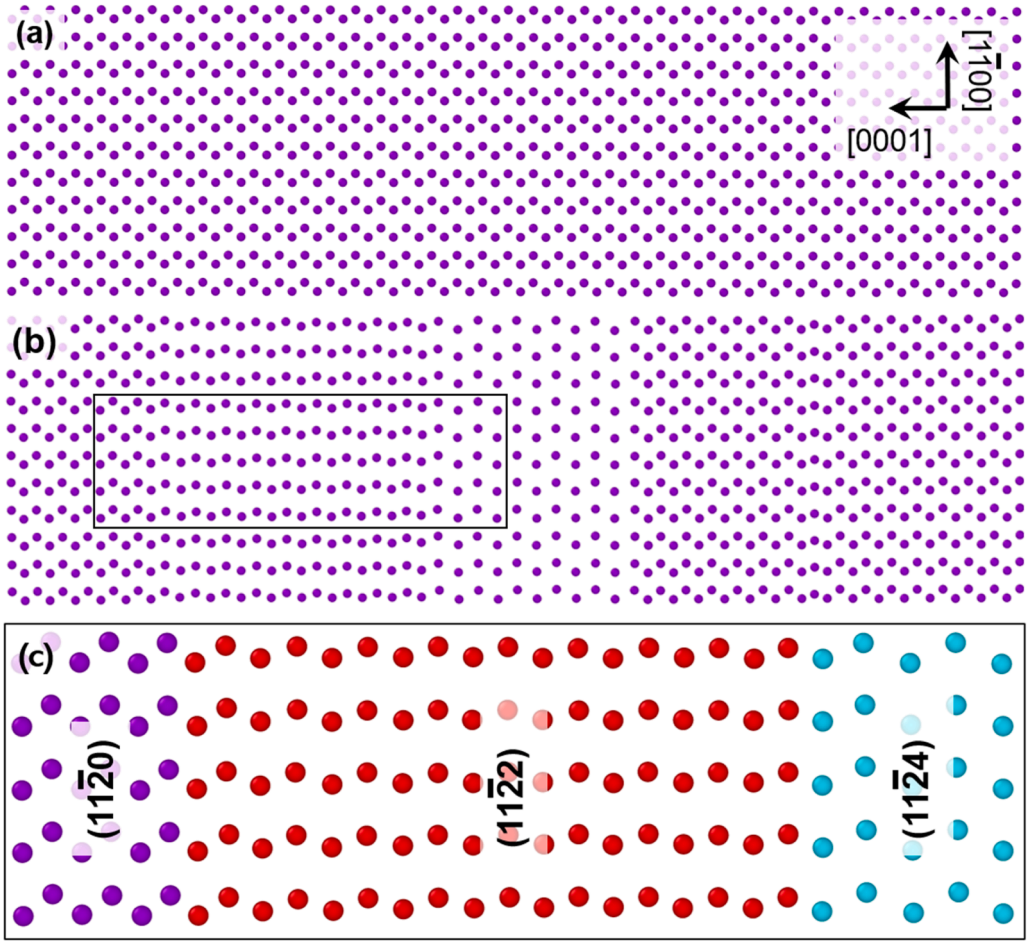

Fig. 9. (a) The pre-selected purple (11$\bar{2}$0) plane in Fig. 8b is viewed down roughly along the plane normal. No twinning has happened. (b) The structure of the purple plane after the (11$\bar{2}$1) twins and the (11$\bar{2}$2) twin are formed. The purple plane now spans over the lattice of the G2, $(11\bar{2}1)_{T2}$ and (11$\bar{2}$2) twin. The boxed region is selected to compare the lattice structure of the initial and the twinned regions. (c) The (11$\bar{2}$0) portion, (11$\bar{2}$2) portion and (11$\bar{2}$4) portion of the pre-selected plane are highlighted and colored in purple, red and cyan, respectively. A structural similarity between these corresponding planes can clearly be seen. The initial (11$\bar{2}$0) plane has to be stretched to form the (11$\bar{2}$2) and the (11$\bar{2}$4) plane.

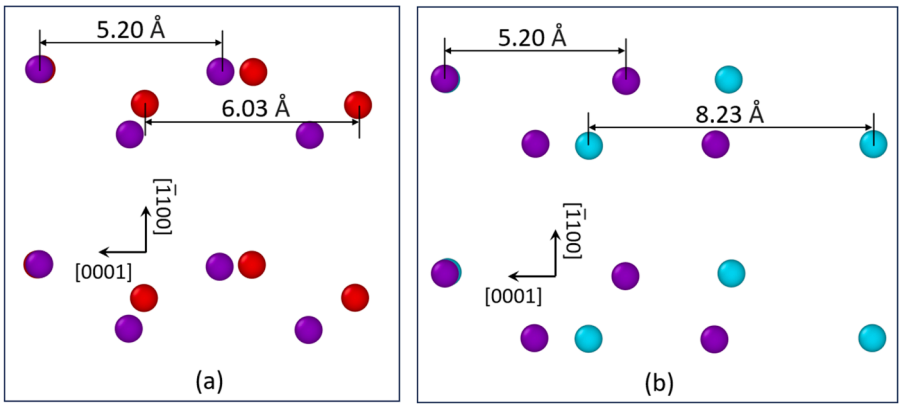

Fig. 10. (a) Comparison between the structure of $(11\bar{2}0)$ (in purple) and $(11\bar{2}2)$ (in red). The two planes are superimposed and aligned along the $[\bar{1}100]$ direction. The misfit strain along the [0001] is ~0.16. (b) The misfit strain between $(11\bar{2}0)$ (in purple) and $(11\bar{2}4)$ (in cyan) is ~0.58. This may explain why direct transformation from the $(11\bar{2}0)$ to $(11\bar{2}4)$ is rather difficult.

often observed along with $\{10\bar{1}2\}$ twins in electron backscatter diffraction (EBSD) analysis of deformed Ti [64]. This raises a puzzling question as to how $\{11\bar{2}2\}$ twins are nucleated in HCP metals.

Our results reveal a new mechanism for the nucleation of $\{11\bar{2}2\}$ twins in HCP metals, i.e., the twin-twin interaction between co-zone $\{11\bar{2}1\}$ twin variants. Two of the highly mobile $\{11\bar{2}1\}$ TBs may merge into a coherent $\{11\bar{2}2\}$ TB, and the $\{11\bar{2}2\}$ twin grows at the expense of the $\{11\bar{2}1\}$ twin. Such twin-twin interaction is possible for the following reasons. First, the $\{11\bar{2}1\}$ TBs do not have well-defined twinning dislocation line and dislocation core. Minonishi et al. [54] first reported that $\{11\bar{2}1\}$ TBs did not have mirror symmetry. After TB migration, the stacking sequence in the twin differed from that in the parent. This indicates that atomic shuffling must be involved. Li and Chen [18] carefully analyzed the $\{11\bar{2}1\}$ TB structure and found that a symmetric $\{11\bar{2}1\}$ TB would have a much higher energy than an asymmetric TB because the interplanar spacing between the $\{11\bar{2}1\}$ twinning plane, which equals $\frac{\gamma \cdot a}{2\sqrt{4\gamma^2+1}}$, is very small (0.70 Å for Ti and 0.77 Å for Mg) and the high repulsive force between atoms on the mirrored positions forces the atoms to move apart from each other. This leads to the breakdown of the mirror symmetry of the TB. They revealed that each prismatic plane of the parent split into two separated layers and these individual layers recombined with the separated layers from the neighboring prismatic planes into the prismatic planes of the twin. This process involves atomic shuffling in the direction perpendicular to the twinning shear. Analyses of the progression of $\{11\bar{2}1\}$ twin growth showed that the TB was no longer a sharp atomic plane but rather a distorted zone spreading over multiple $\{11\bar{2}1\}$ planes, and no well-defined twinning dislocation lines could be identified. The lack of twinning dislocation lines on the $\{11\bar{2}1\}$ TBs allows the merge of TBs of co-zone twin variants into $\{11\bar{2}2\}$ TBs whose migration is mediated by the single-layer twinning dislocations (Fig. 4). If there were twinning dislocations on the $\{11\bar{2}1\}$ TBs, they would either repel each other or react to form immobile configurations, and the triple junction would be immobile. Second, formation of $\{11\bar{2}2\}$ TBs is energetically favorable. $\{11\bar{2}2\}$ TBs are symmetric, coherent and with minimal lattice distortion. Conceivably, $\{11\bar{2}2\}$ TBs should have a lower energy than incoherent $\{11\bar{2}1\}$ TBs.

It is worth noting that non-co-zone $\{10\bar{1}2\}$ twins can also interact and form interfaces that are close to $\{11\bar{2}2\}$ TBs, as shown by Nave and Barnett [65] and Chen et al. [66]. $\{10\bar{1}2\}$ twin nucleation and growth also do not involve twinning dislocations on the TBs and are mediated purely by atomic shuffles [15,16,67], which has been confirmed by numerous experimental observations and atomistic simulations [62,13,17,68]. Two non-co-zone $\{10\bar{1}2\}$ twin variants are at an orientation relationship (OR) that is close to $\sim 60^\circ\langle 1\bar{1}00\rangle$. This OR is frequently used as a criterion in EBSD to characterize $\{11\bar{2}2\}$ TBs in deformed HCP metals. Indeed, when these variants impinge, the interface between them is very close to a $\{11\bar{2}2\}$ TB, but they are incoherent because a deviation still exists. These interfaces have finite mobility, and eventually the interacting twin variants evolve into a morphology close to $\{11\bar{2}2\}$ twins. More recently, atomistic simulations [69,70] also showed that incoherent interfaces close to $\{11\bar{2}2\}$ TBs could also be formed in Ti through an intermediate phase transformation, i.e., $HCP_{parent} \rightarrow \omega \rightarrow HCP_{twin}$.

The new mechanism for the nucleation of $\{11\bar{2}2\}$ twins is difficult to be observed in polycrystalline bulk materials because the nucleation stage occurs at a very fine scale (a few nanometers). In bulk samples, $\{10\bar{1}2\}\langle 10\bar{1}\bar{1}\rangle$ twinning is the dominant mode. $\{10\bar{1}2\}$, $\{11\bar{2}1\}$ and $\{11\bar{2}2\}$ twins can interact and form very complex twin configurations. However, the nucleation mechanism may be captured by carefully designed *in-situ* HRTEM observations in which the OR of the bicrystal is close to the OR in our simulations. For instance, $\{11\bar{2}1\}$ and $\{11\bar{2}2\}$ twinning were successfully resolved in HCP rhenium on the atomic scale *in-situ* HRTEM experiments conducted by He et al. [71,72]. The mechanisms of these twinning modes were found to be consistent with the atomistic simulations [18,47].

5. Conclusion

In this work, we uncover a new nucleation mechanism for the $\{11\bar{2}2\}\langle 11\bar{2}3\rangle$ twinning mode in HCP Mg and Ti. The following conclusions can be drawn:

(1) A $\{11\bar{2}2\}$ twin may nucleate by twin-twin interaction between $\{11\bar{2}1\}$ variants. When three co-zone $\{11\bar{2}1\}$ twins are formed and interact, two $\{11\bar{2}1\}$ TBs merge into a coherent $\{11\bar{2}2\}$ TB. This is feasible and energetically favorable because the $\{11\bar{2}1\}$ and $\{11\bar{2}2\}$ twins have the same K_2 plane (0001). This $\{11\bar{2}2\}$ twin nucleation does not involve any dislocation reaction in contrast to the twin nucleation mechanisms in cubic structures that are closely related to activities of dissociated lattice dislocations.
(2) After twin nucleation by twin-twin interaction, the growth of $\{11\bar{2}2\}$ twin is mediated by the single-layer twinning dislocations that corresponds to the (0001) K_2 plane. This K_2 plane is consistent with the other atomistic simulations and HRTEM observations.

(3) Lattice correspondence and geometrical analyses indicate that direct nucleation of a $\{11\bar{2}2\}$ twin from the parent lattice would be rather difficult because a fairly large misfit strain (~0.58) between the corresponding planes would be generated. Thus, by forming $\{11\bar{2}1\}$ twin variants as an intermediate step, the misfit strain can be significantly reduced, and the nucleation of $\{11\bar{2}2\}$ twins is facilitated by the twin-twin interaction.

CRediT authorship contribution statement

Yuyang Wang: Writing – original draft, Investigation, Formal analysis, Data curation. **Bin Li:** Writing – review & editing, Supervision, Funding acquisition, Formal analysis, Conceptualization. **Yiliang Liao:** Writing – review & editing, Formal analysis.

Declaration of competing interest

The authors declare that they have no known competing financial interests or personal relationships that could have appeared to influence the work reported in this paper.

Acknowledgments

Bin Li gratefully thanks the support from US National Science Foundation (CMMI-2032483 and 2016263).

Supplementary materials

Supplementary material associated with this article can be found, in the online version, at doi:10.1016/j.actamat.2024.120480.

References

[1] R.V. Mises, Mechanik der plastischen Formänderung von Kristallen, ZAMM J. Appl. Math. Mech. Z. Für Angew. Math. Mech 8 (1928) 161–185, https://doi.org/10.1002/zamm.19280080302.
[2] J.W. Christian, S. Mahajan, Deformation twinning, Prog. Mater. Sci. 39 (1995) 1–157, https://doi.org/10.1016/0079-6425(94)00007-7.
[3] S. Mahajan, G.Y. Chin, Formation of deformation twins in f.c.c. crystals, Acta Metall. 21 (1973) 1353–1363, https://doi.org/10.1016/0001-6160(73)90085-0.
[4] B. Li, B.Y. Cao, K.T. Ramesh, E. Ma, A nucleation mechanism of deformation twins in pure aluminum, Acta Mater. 57 (2009) 4500–4507, https://doi.org/10.1016/j.actamat.2009.06.014.
[5] A.H. Cottrell, B.A. Bilby, LX. A mechanism for the growth of deformation twins in crystals, Philos. Mag. Ser. 42 (1951) 573–581, https://doi.org/10.1080/14786445108561272, 7.
[6] J.F. Nie, K.S. Shin, Z.R. Zeng, Microstructure, deformation, and property of wrought magnesium alloys, Metall. Mater. Trans. A 51 (2020) 6045–6109, https://doi.org/10.1007/s11661-020-05974-z.
[7] N. Li, C. Wang, M.A. Monclús, L. Yang, J.M. Molina-Aldareguia, Solid solution and precipitation strengthening effects in basal slip, extension twinning and pyramidal slip in Mg-Zn alloys, Acta Mater. 221 (2021) 117374, https://doi.org/10.1016/j.actamat.2021.117374.
[8] E.W. Kelley, W.F. Hosford, Plane-strain compression of magnesium and magnesium alloy crystals, Trans. Metall. Soc. AIME 242 (1968) 5–13.
[9] J.F. Nie, K.S. Shin, Z.R. Zeng, Microstructure, deformation, and property of wrought magnesium alloys, Metall. Mater. Trans. A 51 (2020) 6045–6109, https://doi.org/10.1007/s11661-020-05974-z.
[10] N. Thompson, D.J. Millard, Twin formation, in cadmium, Philos. Mag. Ser. 43 (1952) 422–440, https://doi.org/10.1080/14786440408520175, 7.
[11] S. Mendelson, Zonal dislocations and twin lamellae in h.c.p. metals, Mater. Sci. Eng. 4 (1969) 231–242, https://doi.org/10.1016/0025-5416(69)90067-6.
[12] B. Li, E. Ma, Zonal dislocations mediating {10-11}<10−1-2>twinning in magnesium, Acta Mater. 57 (2009) 1734–1743, https://doi.org/10.1016/j.actamat.2008.12.016.
[13] S.G. Song, G.T. Gray, Structural interpretation of the nucleation and growth of deformation twins in Zr and Ti—I. Application of the coincidence site lattice (CSL) theory to twinning problems in h.c.p. structures, Acta Metall. Mater. 43 (1995) 2325–2337, https://doi.org/10.1016/0956-7151(94)00433-1.
[14] S.G. Song, G.T. Gray, Structural interpretation of the nucleation and growth of deformation twins in Zr and Ti—II. Tem study of twin morphology and defect reactions during twinning, Acta Metall. Mater. 43 (1995) 2339–2350, https://doi.org/10.1016/0956-7151(94)00434-X.
[15] B. Li, E. Ma, Atomic shuffling dominated mechanism for deformation twinning in magnesium, Phys. Rev. Lett. 103 (2009) 035503, https://doi.org/10.1103/PhysRevLett.103.035503.
[16] X.Y. Zhang, B. Li, X.L. Wu, Y.T. Zhu, Q. Ma, Q. Liu, P.T. Wang, M.F. Horstemeyer, Twin boundaries showing very large deviations from the twinning plane, Scr. Mater. 67 (2012) 862–865, https://doi.org/10.1016/j.scriptamat.2012.08.012.
[17] B.Y. Liu, J. Wang, B. Li, L. Lu, X.Y. Zhang, Z.W. Shan, J. Li, C.L. Jia, J. Sun, E. Ma, Twinning-like lattice reorientation without a crystallographic twinning plane, Nat. Commun. 5 (2014), https://doi.org/10.1038/ncomms4297.
[18] B. Li, K. Chen, Asymmetric (11-21)[11-2-6] twin boundary and migration mechanism in hexagonal close-packed titanium, Acta Mater. 232 (2022) 117943, https://doi.org/10.1016/j.actamat.2022.117943.
[19] S. Vaidya, S. Mahajan, Accommodation and formation of {11-21} twins in Co single crystals, Acta Metall. 28 (1980) 1123–1131, https://doi.org/10.1016/0001-6160(80)90095-4.
[20] J. Wang, S.K. Yadav, J.P. Hirth, C.N. Tomé, I.J. Beyerlein, Pure-shuffle nucleation of deformation twins in hexagonal-close-packed metals, Mater. Res. Lett. 1 (2013) 126–132, https://doi.org/10.1080/21663831.2013.792019.
[21] B.Y. Liu, Z. Zhang, F. Liu, N. Yang, B. Li, P. Chen, Y. Wang, J.H. Peng, J. Li, E. Ma, Z.W. Shan, Rejuvenation of plasticity via deformation graining in magnesium, Nat. Commun. 13 (2022) 1060, https://doi.org/10.1038/s41467-022-28688-9.
[22] B. Li, K. Chen, Grain boundary migration facilitated by phase transformation and twinning in face-centered cubic metals, J. Mater. Sci. 58 (2023) 14740–14757, https://doi.org/10.1007/s10853-023-08863-z.
[23] P. Hirel, Atomsk: a tool for manipulating and converting atomic data files, Comput. Phys. Commun. 197 (2015) 212–219, https://doi.org/10.1016/j.cpc.2015.07.012.
[24] M. Niewczas, Lattice correspondence during twinning in hexagonal close-packed crystals, Acta Mater. 58 (2010) 5848–5857, https://doi.org/10.1016/j.actamat.2010.06.059.
[25] K. Dang, S. Wang, M. Gong, R.J. McCabe, J. Wang, L. Capolungo, Formation and stability of long basal-prismatic facets in Mg, Acta Mater. 185 (2020) 119–128, https://doi.org/10.1016/j.actamat.2019.11.070.
[26] P.G. Partridge, E. Roberts, The formation and behaviour of incoherent twin boundaries in hexagonal metals, Acta Metall. 12 (1964) 1205–1210, https://doi.org/10.1016/0001-6160(64)90103-8.
[27] G.J. Ackland, M.I. Mendelev, D.J. Srolovitz, S. Han, A.V. Barashev, Development of an interatomic potential for phosphorus impurities in α-iron, J. Phys. Condens. Matter 16 (2004) S2629–S2642.
[28] M.I. Mendelev, G.J. Ackland, Development of an interatomic potential for the simulation of phase transformations in zirconium, Philos. Mag. Lett. 87 (2007) 349–359, https://doi.org/10.1080/09500830701191393.
[29] M.S. Daw, M.I. Baskes, Embedded-atom method: derivation and application to impurities, surfaces, and other defects in metals, Phys. Rev. B 29 (1984) 6443–6453, https://doi.org/10.1103/PhysRevB.29.6443.
[30] A. Stukowski, Visualization and analysis of atomistic simulation data with OVITO-the open visualization tool, Model. Simul. Mater. Sci. Eng. 18 (2010) 015012, https://doi.org/10.1088/0965-0393/18/1/015012.
[31] M.W. Finnis, J.E. Sinclair, A simple empirical N-body potential for transition metals, Philos. Mag. A 50 (1984) 45–55, https://doi.org/10.1080/01418618408244210.
[32] X.Y. Liu, J.B. Adams, Grain-boundary segregation in Al–10%Mg alloys at hot working temperatures, Acta Mater. 46 (1998) 3467–3476, https://doi.org/10.1016/S1359-6454(98)00038-X.
[33] B. Li, E. Ma, Zonal dislocations mediating $\{10\bar{1}1\}\langle 10\bar{1}2\rangle$ twinning in magnesium, Acta Mater. 57 (2009) 1734–1743, https://doi.org/10.1016/j.actamat.2008.12.016.
[34] B. Li, E. Ma, Pyramidal slip in magnesium: dislocations and stacking fault on the 1011 plane, Philos. Mag. 89 (2009) 1223–1235, https://doi.org/10.1080/14786430902936707.
[35] B. Li, Q.W. Zhang, S.N. Mathaudhu, Basal-pyramidal dislocation lock in deformed magnesium, Scr. Mater. 134 (2017) 37–41, https://doi.org/10.1016/j.scriptamat.2017.02.040.
[36] D.Y. Sun, M.I. Mendelev, C.A. Becker, K. Kudin, T. Haxhimali, M. Asta, J.J. Hoyt, A. Karma, D.J. Srolovitz, Crystal-melt interfacial free energies in hcp metals: a molecular dynamics study of Mg, Phys. Rev. B 73 (2006) 024116, https://doi.org/10.1103/PhysRevB.73.024116.
[37] S.R. Wilson, M.I. Mendelev, A unified relation for the solid-liquid interface free energy of pure FCC, BCC, and HCP metals, J. Chem. Phys. 144 (2016) 144707, https://doi.org/10.1063/1.4946032.
[38] Y.M. Kim, N.J. Kim, B.J. Lee, Atomistic Modeling of pure Mg and Mg–Al systems, Calphad 33 (2009) 650–657, https://doi.org/10.1016/j.calphad.2009.07.004.
[39] D. Dickel, M. Nitol, C.D. Barrett, LAMMPS implementation of rapid artificial neural network derived interatomic potentials, Comput. Mater. Sci. 196 (2021) 110481, https://doi.org/10.1016/j.commatsci.2021.110481.
[40] M.S. Nitol, S. Mun, D.E. Dickel, C.D. Barrett, Unraveling Mg $\langle c + a\rangle$ slip using neural network potential, Philos. Mag. 102 (2022) 651–673, https://doi.org/10.1080/14786435.2021.2012289.
[41] D.Y. Sun, M.I. Mendelev, C.A. Becker, K. Kudin, T. Haxhimali, M. Asta, J.J. Hoyt, A. Karma, D.J. Srolovitz, Crystal-melt interfacial free energies in hcp metals: a molecular dynamics study of Mg, Phys. Rev. B 73 (2006) 024116, https://doi.org/10.1103/PhysRevB.73.024116.
[42] S.R. Wilson, M.I. Mendelev, A unified relation for the solid-liquid interface free energy of pure FCC, BCC, and HCP metals, J. Chem. Phys. 144 (2016) 144707, https://doi.org/10.1063/1.4946032.

[43] M.I. Baskes, Modified embedded-atom potentials for cubic materials and impurities, Phys. Rev. B 46 (1992) 2727–2742, https://doi.org/10.1103/PhysRevB.46.2727.
[44] Y.M. Kim, N.J. Kim, B.J. Lee, Atomistic Modeling of pure Mg and Mg–Al systems, Calphad 33 (2009) 650–657, https://doi.org/10.1016/j.calphad.2009.07.004.
[45] J.Dana. Honeycutt, H.C. Andersen, Molecular dynamics study of melting and freezing of small Lennard-Jones clusters, J. Phys. Chem. 91 (1987) 4950–4963, https://doi.org/10.1021/j100303a014.
[46] H. Zhang, X. Ou, S. Ni, H. Yan, X. Liao, M. Song, Atomic-scale study of the {112¯1} twinning and {112¯2}-{112¯1} double twinning mechanisms in pure titanium, Int. J. Plast. 160 (2023) 103486, https://doi.org/10.1016/j.ijplas.2022.103486.
[47] J. Li, M. Sui, B. Li, A half-shear-half-shuffle mechanism and the single-layer twinning dislocation for {11-22}⟨11-2-3⟩ mode in hexagonal close-packed titanium, Acta Mater. 216 (2021) 117150, https://doi.org/10.1016/j.actamat.2021.117150.
[48] N. Stanford, D. Atwell, M.R. Barnett, The effect of Gd on the recrystallisation, texture and deformation behaviour of magnesium-based alloys, Acta Mater. 58 (2010) 6773–6783, https://doi.org/10.1016/j.actamat.2010.09.003.
[49] N. Ansari, S.Y. Lee, S.S. Singh, J. Jain, Influence of yttrium-induced twinning on the recrystallization behavior of magnesium alloys, J. Mater. Sci. 56 (2021) 18258–18271, https://doi.org/10.1007/s10853-021-06418-8.
[50] N. Stanford, Observation of 1121 twinning in a Mg-based alloy, Philos. Mag. Lett. 88 (2008) 379–386, https://doi.org/10.1080/09500830802070793.
[51] H. Fan, J.A. El-Awady, Molecular dynamics simulations of orientation effects during tension, compression, and bending deformations of magnesium nanocrystals, J. Appl. Mech. (2015) 82, https://doi.org/10.1115/1.4030930.
[52] P. Chen, J. Ombogo, B. Li, Dislocation ↔ twin transmutations during interaction between prismatic slip and {101¯1} twin in magnesium, Acta Mater 186 (2020) 291–307, https://doi.org/10.1016/j.actamat.2020.01.010.
[53] B.A. Bilby, A.G. Crocker, The theory of the crystallography of deformation twinning, Proc. R. Soc. Lond. Ser. Math. Phys. Sci. 288 (1965) 240–255, https://doi.org/10.1098/rspa.1965.0216.
[54] Y. Minonishi, S. Ishioka, M. Koiwa, S. Mobozumi, The structure of {1121} twin boundaries in H.C.P. crystals, Phys. Status Solidi A 71 (1982) 253–258, https://doi.org/10.1002/pssa.2210710130.
[55] B. Li, Reply to the two comments, by A. Serra, D.J. Bacon and R.C. Pond, and by H. El Kadiri and C. Barrett on B. Li, H. El Kadiri and M.F. Horstemeyer "Extended zonal dislocations mediating twinning in titanium, Philos. Mag. 93 (2013) 3504–3510, https://doi.org/10.1080/14786435.2013.815818.
[56] J.W. Christian, The Theory of Transformations in Metals and Alloys, Newnes, 2002.
[57] B. Li, H. El Kadiri, M.F. Horstemeyer, Extended zonal dislocations mediating twinning in titanium, Philos. Mag. 92 (2012) 1006–1022, https://doi.org/10.1080/14786435.2011.637985.
[58] S. Kibey, J.B. Liu, D.D. Johnson, H. Sehitoglu, Predicting twinning stress in fcc metals: linking twin-energy pathways to twin nucleation, Acta Mater. 55 (2007) 6843–6851, https://doi.org/10.1016/j.actamat.2007.08.042.
[59] K.T. Hsieh, Y.Y. Lin, C.H. Lu, J.R. Yang, P.K. Liaw, C.L. Kuo, Atomistic simulations of the face-centered-cubic-to-hexagonal-close-packed phase transformation in the equiatomic CoCrFeMnNi high entropy alloy under high compression, Comput. Mater. Sci. 184 (2020) 109864, https://doi.org/10.1016/j.commatsci.2020.109864.
[60] X.L. Wu, X.Z. Liao, S.G. Srinivasan, F. Zhou, E.J. Lavernia, R.Z. Valiev, Y.T. Zhu, New deformation twinning mechanism generates zero macroscopic strain in nanocrystalline metals, Phys. Rev. Lett. 100 (2008) 095701, https://doi.org/10.1103/PhysRevLett.100.095701.
[61] Y.T. Zhu, X.Z. Liao, X.L. Wu, Deformation twinning in nanocrystalline materials, Prog. Mater. Sci. 57 (2012) 1–62, https://doi.org/10.1016/j.pmatsci.2011.05.001.
[62] Y. He, B. Li, C. Wang, S.X. Mao, Direct observation of dual-step twinning nucleation in hexagonal close-packed crystals, Nat. Commun. 11 (2020) 2483, https://doi.org/10.1038/s41467-020-16351-0.
[63] Q. Yu, Z.W. Shan, J. Li, X. Huang, L. Xiao, J. Sun, E. Ma, Strong crystal size effect on deformation twinning, Nature 463 (2010) 335–338, https://doi.org/10.1038/nature08692.
[64] F. Xu, X. Zhang, H. Ni, Y. Cheng, Y. Zhu, Q. Liu, Effect of twinning on microstructure and texture evolutions of pure Ti during dynamic plastic deformation, Mater. Sci. Eng. A 564 (2013) 22–33, https://doi.org/10.1016/j.msea.2012.11.097.
[65] M.D. Nave, M.R. Barnett, Microstructures and textures of pure magnesium deformed in plane-strain compression, Scr. Mater. 51 (2004) 881–885, https://doi.org/10.1016/j.scriptamat.2004.07.002.
[66] P. Chen, F. Wang, J. Ombogo, B. Li, Formation of 60°⟨01-10⟩ boundaries between {10-12} twin variants in deformation of a magnesium alloy, Mater. Sci. Eng. A 739 (2019) 173–185, https://doi.org/10.1016/j.msea.2018.10.029.
[67] B. Li, X.Y. Zhang, Twinning with zero twinning shear, Scr. Mater. 125 (2016) 73–79, https://doi.org/10.1016/j.scriptamat.2016.07.004.
[68] B. Li, X.Y. Zhang, Global strain generated by shuffling-dominated twinning, Scr. Mater. 71 (2014) 45–48, https://doi.org/10.1016/j.scriptamat.2013.10.002.
[69] J. Ombogo, A.H. Zahiri, T. Ma, L. Cao, Nucleation of {1012} twins in magnesium through reversible martensitic phase transformation, Metals 10 (2020) 1030, https://doi.org/10.3390/met10081030 (Basel).
[70] A.H. Zahiri, J. Ombogo, L. Cao, Formation of {112¯2} contraction twins in titanium through reversible martensitic phase transformation, Scr. Mater. 195 (2021) 113694, https://doi.org/10.1016/j.scriptamat.2020.113694.
[71] Y. He, Atomic-Scale *in Situ* Tem Investigation of Deformation Twinning in Hcp Crystals, University of Pittsburgh, 2018.
[72] Y. He, Z. Fang, C. Wang, G. Wang, S.X. Mao, *In situ* observation of the atomic shuffles during the {11-21} twinning in hexagonal close-packed rhenium, Nat. Commun. 15 (2024) 2994, https://doi.org/10.1038/s41467-024-47343-z.